



CHORUS

This is the accepted manuscript made available via CHORUS. The article has been published as:

Quantum Properties of Dichroic Silicon Vacancies in Silicon Carbide

Roland Nagy, Matthias Widmann, Matthias Niethammer, Durga B. R. Dasari, Ilja Gerhardt, Öney O. Soykal, Marina Radulaski, Takeshi Ohshima, Jelena Vučković, Nguyen Tien Son, Ivan G. Ivanov, Sophia E. Economou, Cristian Bonato, Sang-Yun Lee, and Jörg Wrachtrup

Phys. Rev. Applied **9**, 034022 — Published 23 March 2018

DOI: [10.1103/PhysRevApplied.9.034022](https://doi.org/10.1103/PhysRevApplied.9.034022)

Quantum properties of dichroic silicon vacancies in silicon carbide

Roland Nagy,^{1†} Matthias Widmann,^{1†} Matthias Niethammer,¹ Durga B.R. Dasari,¹ Ilja Gerhardt,^{1,2} Öney O. Soykal,³ Marina Radulaski,⁴ Takeshi Ohshima,⁵ Jelena Vučković,⁴ Nguyen Tien Son,⁶ Ivan G. Ivanov,⁶ Sophia E. Economou,⁷ Cristian Bonato,⁸ Sang-Yun Lee,^{9*} Jörg Wrachtrup^{1,2}

¹*3. Institute of Physics, University of Stuttgart and Center for Integrated Quantum Science and Technology, IQST, Pfaffenwaldring 57, D-70569 Stuttgart, Germany*

²*Max Planck Institute for Solid State Research, Heisenbergstrasse 1, D-70569 Stuttgart, Germany*

³*Naval Research Laboratory, Washington, DC 20375, USA*

⁴*E. L. Ginzton Laboratory, Stanford University, Stanford, California 94305, USA*

⁵*National Institutes for Quantum and Radiological Science and Technology, Takasaki, Gunma 370-1292, Japan*

⁶*Department of Physics, Chemistry, and Biology, Linköping University, SE-58183 Linköping, Sweden*

⁷*Department of Physics, Virginia Polytechnic Institute & State University, Blacksburg, VA 24061, USA*

⁸*Institute of Photonics and Quantum Sciences, SUPA, Heriot-Watt University, Edinburgh EH14 4AS, UK*

⁹*Center for Quantum Information, Korea Institute of Science and Technology, Seoul, 02792, Republic of Korea*

Although various defect centers have displayed promise as either quantum sensors, single photon emitters or light-matter interfaces, the search for an ideal defect with multi-functional ability remains open. In this spirit, we study the dichroic silicon vacancies in silicon carbide that feature two well-distinguishable zero-phonon lines and analyze the quantum properties in their optical emission and spin control. We demonstrate that this center combines 40% optical emission into the zero-phonon line showing the contrasting difference in optical properties with varying temperature and polarization, and 100% increase in the fluorescence intensity upon the spin resonance, and long spin coherence time of their spin-3/2 ground states up to 0.6 ms. These results single out this defect center as a promising system for spin-based quantum technologies.

I. INTRODUCTION

Quantum technologies based on solid-state devices can take advantage of well-established fabrication and control methods developed over the past century. Among several quantum systems, color centers in diamond [1–3] have gained prominence as quantum-enhanced nanoscale sensors [4], coherent spin-photon/phonon interfaces [5–7] and quantum registers [8]. Despite their success, the limited emission rate of indistinguishable photons of e.g. the nitrogen vacancy (NV) center and the difficulties of diamond nanofabrication currently inhibit the progress towards efficient and scalable spin-photon interfacing devices [9] which is a prerequisite for building quantum networks and network-based quantum computing devices. Defect spins in silicon carbide (SiC) have been studied as an analog to diamond color centers, due to their promising complementary properties and the established technologies in growth, doping and device fabrication [10]. As in diamond, defect spins in SiC exhibit long coherence times [11–13] and optically detectable spin signals at room temperatures [14–16], down to the individual spin level [17,18]. SiC hosts several defects with addressable electronic spins, including silicon vacancies [13,18], divacancies [12,17], and transition metal impurities [19,20].

II. DICHOIC SILICON VACANCY

The silicon vacancy (V_{Si}) in SiC is one of the naturally occurring point defects [21] and can be created by kicking out silicon atoms using accelerated particles [14]. There have been two competing models for their atomic structure, an isolated negatively charged V_{Si} [21,22] and a V_{Si} bonded to a neutral carbon vacancy [16,23], for the precise identity of V_{Si} . While most defects in semiconductors used in quantum technology host a $S=1/2$ or 1 electronic spins [3,20,22,24], the silicon vacancy (V_{Si}) in hexagonal SiC features a $S=3/2$ electronic spin in uniaxial crystal lattices. Its ground state was assigned as $S=1$ [14] but identified as $S=3/2$ by many experimental evidences [23,25–27]. According to Kramers' theorem [28], the degeneracy of a half-integer spin system can only be broken by magnetic fields, making it insensitive to fluctuations in strain, temperature, and electric field. Furthermore, the same Landé g -factor of ground and excited states makes the optical transitions corresponding to different spin states spectrally indistinguishable, for any applied magnetic

field [21]. These factors have led to a theoretical proposal, by Soykal *et al.* [29,30], of a robust interface between spin and photon polarization, which is not perturbed by environmental noise. Additionally, while other defects exist in several different orientations in the crystal lattice [31,32], V_{Si} at each inequivalent lattice exhibit only one single spin orientation along the c-axis of the crystal [14,16]. This can allow deterministic orientation, enhancing scalability in devices. In this work, we demonstrate that the V1 center, one of the two V_{Si} centers residing at two inequivalent lattice sites of in 4H-SiC [21], features a large fraction of radiation into the zero-phonon-lines (ZPL) of up to 40%. In addition, two sharp ZPLs exhibit contrasting polarization properties which may pave a new way for quantum control. To discriminate the V1 center with the V2 center whose ZPL is known to be monochromatic, we call it “dichroic silicon vacancy” through this report. These properties can form the basis of the robust spin-photon interface [29]. We also demonstrate efficient spin polarization and readout resulting in nearly 100% relative increase in optically detected spin signal allowing the high-fidelity spin state readout, and long spin coherence time into the millisecond range. We conclude with some considerations about the prospects to realize a robust spin-photon interface [29,30]. While the V2 center has been intensively studied in the context of quantum applications [13,18,23,27,33–35], there are only a small number of prior studies for V1 center mostly due to the absence of spin resonance signals at the elevated temperatures [14,21,33].

III. MATERIALS AND METHODS

All measurements were performed on a commercially available high purity 4H-SiC substrate. The sample was electron irradiated (2 MeV) with a dose of 5×10^{17} electrons/cm² to create a high density of V_{Si} defect centers. The sample was placed in a closed-cycle cryostat from Montana instruments, at a temperature around 5K. A static magnetic field $B_0 = 60$ and $B_0 = 1000$ G was applied parallel to the c-axis by a permanent magnet. Optical excitation was performed either resonantly, by a 858/861 nm laser diode using a Littrow external cavity or off-resonantly by a 730nm laser diode. The light was focused on the sample by a high NA (0.9) air objective. The RF/MW fields were created by a vector signal generator (Rhode & Schwartz SMIQ 06B), amplified by a 30 W amplifier (Mini-Circuits, LZY – 22+). Radio-frequency (RF) fields were delivered by a copper

wire with a diameter of 20 μm , which was spanned on the sample surface. Further information can be found in the Supplemental Materials [36].

IV. FLUORESCENCE PROPERTIES

The theoretical energy-level scheme, proposed by the group-theoretical analysis, is sketched in Fig. 1(a). The ground state of V1 is a spin quartet of symmetry ${}^4A_2(a_1^2a_1^1e^2)$ and total spin $S=3/2$ [21]. The ground $|\pm 1/2\rangle$ and $|\pm 3/2\rangle$ sublevels of V1 are split by a zero-field splitting (ZFS) of 4 MHz [21]. Two excited states ${}^4E(a_1^1a_1^1e^3)$ and ${}^4A_2(a_1^2a_1^1e^2)$ can be selectively excited from the ground state via resonant laser excitation with 1.445 eV (858 nm) and 1.440 eV (861 nm), known as V1' and V1 ZPLs, respectively [21,37]. At a temperature of 5.5 K, both the emission of the V1 ZPL transition (4A_2 to 4A_2) and V1' ZPL emission (4E to 4A_2) are observable as shown in Fig. 1(b) and their decay times, the excited state lifetimes, are approximately 6 ns [36]. Their intensities show temperature dependence, i.e. V1' ZPL intensity peaks at around 70 K (Fig. 1(b)). The energy difference between the ZPLs of V1 and V1' is about 4.4 meV which corresponds to a thermodynamic equivalent temperature of 51 K. The enhanced emission from the V1' transition at elevated temperatures may be understood as a phonon-assisted process [36].

The protocol by Soykal *et al.* for a robust spin-photon interface features the energetically degenerate but orthogonally polarized photons [29,30] associated to V1. Here we report a complete characterization of the polarization properties of V1' and V1 ZPL. While some polarization studies were reported in the literature [21,38], we will show that the current model for this defect requires revision. The polar plot in Fig. 1(c) represents the integrated intensity of each of the V1 and V1' ZPLs as a function of the half-wave plate angle, taken at $T=5.5$ K with the laser incident angle perpendicular to the c-axis. The dominant polarizations of V1 and V1' ZPLs are almost orthogonal to each other. The full orientation analysis results are in qualitative agreement with previously suggested optical selection rules based on group-theoretical analysis within the single group C_{3v} , representing the symmetry of V_{Si} [21,38]. This analysis predicts $\mathbf{E} \parallel \mathbf{c}$ polarization for the V1

transition and $\mathbf{E} \perp \mathbf{c}$ polarization for the V1' transition. However, while the photons originating from V1' are quite well linearly polarized $\mathbf{E} \perp \mathbf{c}$, the V1 transition is not entirely polarized as $\mathbf{E} \parallel \mathbf{c}$ but contains a component $\mathbf{E} \perp \mathbf{c}$. These indicate that the selection rules need revision. Since the negatively-charged V_{Si} contains an odd number of electrons (resulting in half-integer spin), the correct symmetry is the double group $\overline{C_{3v}}$, as previously suggested [29]. The derivation of the selection rules for $\overline{C_{3v}}$ leads to a better estimate of the relative contribution of the $\mathbf{E} \parallel \mathbf{c}$ and $\mathbf{E} \perp \mathbf{c}$ polarizations in the optical emission of the V1 and V1' ZPLs. This is outlined in the Supplemental Materials [36]. We find that for the V1 transition the distribution among the two polarizations is $\mathbf{E} \parallel \mathbf{c} : \mathbf{E} \perp \mathbf{c} = 3:1$, whereas for the V1' transition the proportion is $\mathbf{E} \perp \mathbf{c} : \mathbf{E} \parallel \mathbf{c} = 11:1$. These estimates are in good agreement with the polar plots in Fig. 1(c), $\mathbf{E} \parallel \mathbf{c} / \mathbf{E} \perp \mathbf{c} = 1.85 \pm 0.06$ for V1, and $\mathbf{E} \perp \mathbf{c} / \mathbf{E} \parallel \mathbf{c} = 19 \pm 3$ for V1'. For completeness, polarization is also measured with the laser incident angle parallel to the c-axis [36].

V. OPTICAL SPIN STATE DETECTION

In the next set of measurements, we characterize the spin properties for a defect ensemble. The ground state spin can be polarized into the sublevels $|S_z = \pm 3/2\rangle$ [29] by optical pumping [33] with an off-resonant laser ($\lambda = 730$ nm). At any constant finite magnetic fields (B_0), the spin energy levels are determined by the Hamiltonian,

$$H = g\mu_B \mathbf{B} \cdot \mathbf{S} + D[S_z^2 - S(S+1)/3], \quad (1)$$

where g is the Landé g -factor, μ_B is the Bohr magneton, D is the ZFS ($2D = 4$ MHz), and S_z is the projection the total spin onto the quantization axis, the c-axis in 4H-SiC. By applying resonant radio-frequency (RF) fields (B_1) one can induce transitions between spin sublevels (Fig. 2(a)), resulting in a change in optically detected magnetic resonance (ODMR) as shown in Fig. 2(b). The relative change in ODMR signal is calculated as $[I(f) - I_{off}] / I_{off}$, where $I(f)$ is the PL intensity at the RF frequency f , and I_{off} is the PL intensity at the off-resonant RF frequency. The spin-sublevels are energetically split at $B_0 = 60$ G aligned along the c-axis. The relative ODMR signal as a function of the driving RF frequency shows a negative signal at 170 MHz, with the

relative intensity 0.05% as in the upper panel of Fig. 2(b). It is attributed to the V1 ground state spin; a similar signal was also reported for V1 and V3 centers in 6H-SiC [33]. By exciting the optical transition V1 resonantly as in Fig.1(a) a positive relative ODMR signal with $100 \pm 0.6\%$ is achieved (lower panel in Fig. 2(b)). In contrast, excitation of the V1' optical transition in Fig.1(a) reveals a negative signal with a minimal increase in the relative signal intensity [36]. A similar substantial enhancement of the ODMR signal was reported for the V2 center ensemble in 6H-SiC [33]. Although the underlying mechanism is not yet completely understood, we attribute it to the enhanced spin polarization in the ground state resulting from resonant optical excitation. Resonant excitation of V1 ZPL results in the excitation into the lowest vibrational level of the V1 excited state. This efficiently suppresses the phonon-assisted spin-mixing between the 4A_2 and 4E excited states leading to an improvement in the ODMR signal at sufficiently low temperatures ($k_B T < 4.4$ meV). On the other hand, resonant excitation of V1' does not result in such an improvement as it still involves the excitation of V1 (lower in energy) and its vibrational levels. This observation may also indicate that optical polarization is mainly established by the intersystem-crossing (ISC) between the 4A_2 excited states and the 2E metastable state while the 4E excited states have a less efficient ISC [29]. We expect further enhancement of the ODMR signal when a single V1 center is isolated owing to the suppressed inhomogeneous broadening. We note that if an identical ODMR contrast, namely C , and an identical photoluminescence (PL) intensity without spin resonance are assumed, a positive signal leads to a signal-to-noise ratio larger than the negative signal, as of the NV center in diamond [1] and divacancies in 4H- and 6H-SiC [32], by a factor of $(1 - C)^{-0.5}$ [36].

VI. COHERENT SPIN CONTROL

In order to demonstrate coherent control of the electronic spins, we investigated spin dynamics of the V1 center ensemble under applied RF pulses. The resulting distribution of the Rabi oscillations in the range of $f = 160$ -190 MHz at $B_0 = 60$ G, is shown in Fig. 3(a). The dynamics is strikingly different from the single-frequency Rabi oscillations typical of a two-level system. Further understanding can be obtained by plotting the Fast-Fourier transform of the Rabi oscillations, for different values of the driving power. For two-level

transitions one expects parabolic profiles, corresponding to a Rabi frequency Ω increasing with the detuning $\Delta\omega$ as $\Omega^2 = \Omega_0^2 + \Delta\omega^2$ where Ω_0 is the driving frequency determined by the applied B_1 field strength ($\Omega_0 \propto B_1$). The experimental data reveal richer and more complex dynamics. We explain our observations with the presence of three closely-spaced transitions, corresponding to f_1 , f_2 , and f_3 in Fig. 2(a). While resonantly driving one transition, due to the small ZFS, off-resonant excitation of the other two transitions is not negligible. To support this explanation, we developed a theoretical model based on four levels of S=3/2 driven by a single monochromatic radio-frequency field. The system dynamics is investigated assuming initial polarization into an incoherent mixture of $|S_z = \pm 3/2\rangle$. Further details on the model can be found in the Supplemental Materials [36]. Our simulations match quite closely the complex structure of the experimental data (see Figure 3(c, d)). When f is lower than f_1 ($|-3/2\rangle \leftrightarrow |-1/2\rangle$), the transition f_1 is mainly excited, leading to a parabolic profile. However, off-resonant excitation of the transition f_2 , coupling $|-1/2\rangle$ to $|+1/2\rangle$, results in a second weaker Fourier component in the Rabi spectrum with larger Rabi frequency. With increasing RF power (B_1 field strength), simulated by increasing the driving frequency proportional to the increase of the experimentally used B_1 field strength, this component becomes stronger. When $f=f_2$, one simultaneously drives off-resonantly the transitions f_1 and f_3 , resulting in a larger Rabi frequency. This is evident in the plots corresponding to the largest RF power, where the parabolic profile centered around f_2 shows a much larger Rabi frequency than the profiles related to f_1 and f_3 . Note that the experimental data can only be explained by assuming the excitation of the $|-1/2\rangle \leftrightarrow |+1/2\rangle$ transition, which was not reported. Additionally, the assumption for initial polarization into $|\pm 1/2\rangle$, which is the case for the V2 center, does not reproduce the observed signal. Note that we report for the first time the experimental evidence for S=3/2 of the ground state of the V1 in 4H-SiC [36].

The small ZFS poses challenges for high-fidelity coherent spin control, which need to be addressed for the V1 center to be a serious contender for quantum technology. There are several possibilities to explore: use of (i) optimal quantum control sequences, (ii) adiabatic passage techniques that restrict the dynamics only to a two-level subspace (e.g. $|+3/2\rangle$ and $|-1/2\rangle$), with no leakage to other states of the Hilbert space [39], (iii) pulses designed to avoid a transition by building holes in their frequency spectrum to avoid leakage [40], (iv)

superadiabatic (shortcuts to adiabaticity) control [41], which was recently demonstrated for NV centers in diamond [42]. Alternatively, the V1 in 6H-SiC is known to exhibit a larger ZFS [14,21], which would relax this problem.

VII. SPIN DECOHERENCE

We studied spin coherence at $T = 5.5$ K with $B_0 = 60$ G [36] and 1000 G by Ramsey, Hahn-echo, and XY-8 dynamical decoupling pulse sequences by optical excitation resonant with the V1 ZPL (861 nm). We observed an evolution of the coherent superposition with the electron spin dephasing time of $T_2^* = 1.3 \pm 0.3$ μ s at $B_0 = 1000$ G aligned parallel to the c-axis by a Ramsey experiment as shown in Fig. 4(a). To suppress the inhomogeneous broadening in an ensemble and decouple the spin ensembles from low-frequency spin noise from such as paramagnetic impurities and a nuclear spin bath composed of ^{29}Si and ^{13}C [11], we applied a Hahn-Echo sequence. Identical laser pulses of 2 μ s length were applied before and after the MW pulse sequences for the optical spin polarization and projective spin state readout, respectively, and also to avoid dephasing due to the optical excitation [29]. Although the applied RF pulses exhibit limited spin control to a single transition as discussed in the Supplemental Materials [36], we could see a typical exponential decay with $T_2 = 83.9 \pm 1.6$ μ s (Fig. 4(b)). The observed T_2 is, however, shorter than the theoretical expectations for the V2 center [11] and the value measured for a single V2 center at room temperature [18]. This could be related to the imperfect π pulses and the inhomogeneity of the B_0 field (see the Supplemental Materials [36]). These observations, however, support the findings by Carter *et al.* [34], related to the fact that the dephased state cannot be refocused by a π pulse due to the oscillating local fields produced by coupled nuclear spins. Thus, the shorter T_2 could be related to electron spin echo envelope modulation (ESEEM). The four sublevels of a $S=3/2$ electronic spin have four different non-zero hyperfine coupling to nearby nuclear spins and thus result in more complex ESEEM than $S=1$ systems [11,18]. Furthermore, as reported by Carter *et al.*, the ensemble inhomogeneous broadening induces beating oscillations among the various modulation frequencies, leading to a shortening of the Hahn-echo T_2 [34].

To further suppress decoherence, we applied the XY-8 dynamical decoupling sequence, which acts as a filter for the environmental magnetic noise [43]. This sequence has proven to be effective to extend the coherence time of the $S=3/2$ spin ensemble of the V2 center from the nuclear spin bath in 4H-SiC [13]. A repeated decoupling pulse scheme leads to a better suppression of noise, increasing the spin decoherence time with $N=10$ and $N=50$ repetitions to a value of respectively $T_2 = 286 \pm 7 \mu\text{s}$ and $T_2 = 0.60 \pm 0.01 \text{ ms}$ (Fig. 4(b)). These suggest that the heteronuclear spin bath in SiC itself provides a diluted spin bath for not only the V2 center [13,18], and divacancy defects [17], but also the V1 center.

VIII. ISOLATED SINGLE SILICON VACANCY

Although the spin ensemble-based quantum applications such as quantum memory [44] are valuable, many advanced quantum applications including e.g. the spin-photon interface requires addressing of single defect centers. To test if the single V1 center can be used as an efficient coherent single photon source, e.g. a building-block for the robust spin-photon interface, we isolated single V1 centers in nanopillars fabricated on a 4H-SiC sample [35], as shown in Fig. 5(a). Addressing of a single center is proven by the autocorrelation measurement in a Hanbury Brown and Twiss configuration, with $g^{(2)} < 0.5$ [36]. The saturated count rate of 14 keps was measured by an air objective of $\text{NA}=0.9$ with a single photon detector inefficient in this wavelength (see the Supplemental Materials [36]). The spectrum at $T=4\text{K}$ shows both V1 and V1' ZPLs as in Fig. 5(b), further proof that they correspond to two different excited states of the same defect. To determine the Debye-Waller factor (DWF), the fraction of radiation into the ZPL of V1 over the whole V1 spectrum, the contribution of V1' to the phonon sideband (PSB) has to be minimized. At 4 K, the intensity of the V1' ZPL is weak, and we suppose that the contribution to the PSB is also negligible in comparison to V1. Then, the conservatively estimated DWF of the V1 is $40 \pm 6 \%$. See the Supplemental Materials [36] for the additional data and DWF of the V1'.

IX. SUMMARY AND OUTLOOK

In summary, optical spectroscopy and polarization measurements confirm the symmetry properties of the V1 center in 4H-SiC, supported by the established double group $\overline{C_{3v}}$ model, substantiating the theoretical model leading to the proposed robust spin-photon interface [29]. A spin-photon interface requires narrow optical transitions [36], weak spectral diffusion and slow spin-flip rates by optical pumping cycles. Recent results on the divacancy in SiC shows that the material quality is sufficiently high to satisfy these requirements [22]. Resonant optical excitation of the V1 ZPL leads to a substantial increase in spin-dependent photoluminescence emission indicating an efficient spin-dependent transition. We also have shown the extension of spin coherence time, through dynamical decoupling sequences, up to 0.6 ms, which will enable long and complex spin manipulation necessary for spin-photon interface [5,45]. While the leading contenders for defect-based quantum spintronics, such as the NV center in diamond and divacancy in 4H-SiC, suffer from low optical emission into zero-phonon lines (with DWF ~3% and 5-7% [22,46], respectively), the V1 center in 4H-SiC features a significantly higher DWF, up to 40%. The high ZPL emission could guarantee a high event rate for the proposed generation of spin-photon entanglement. The weak overall photon emission rate of the V1/V1' transition may be circumvented by using photonic structures fabricated on SiC, which recently have shown progress towards high-Q cavities and efficient photon collection [35,37,47]. This can further be used to generate strings of entangled photons [6,48]. Further work on this dichroic single defect, which is undergoing, is necessary to identify individual optical transitions and the associated selection rules which are essential for realizing spin-photon interfaces, e.g. spin-photon entanglement exploiting transitions to the 4E excited state (V1' line) with the high fidelity spin initialization and read-out with the V1 line.

ACKNOWLEDGEMENT

This work was supported by the ERA.Net RUS Plus Program (DIABASE), the DFG via priority programme 1601, the EU via ERC Grant SMel and Diadems, the Max Planck Society, the Carl Zeiss Stiftung, the Swedish Research Council (VR 2016-04068), the Carl-Trygger Stiftelse för Vetenskaplig Forskning (CTS 15:339), the Knut and Alice Wallenberg Foundation (KAW 2013.0300), the JSPS KAKENHI (A) 17H01056, the National Science Foundation DMR Grant Number 1406028, the U.S. Office of Secretary of Defense Quantum Science and Engineering Program, the COST Action MP1403 “Nanoscale Quantum Optics” funded by COST (European Cooperation in Science and Technology), and by EPSRC (grant EP/P019803/1), the Army Research Office under contract W911NF1310309, and the KIST Open Research Program (2E27231) and institutional program (2E27110). We thank Roman Kolesov, Rainer Stöhr, and Torsten Rendler for fruitful discussions and experimental aid. We also acknowledge motivating discussions with Michel Bockstedte, Adam Gali, Thomas L. Reinecke, and Jingyuan Linda Zhang. We thank Rainer Stöhr for proofreading.

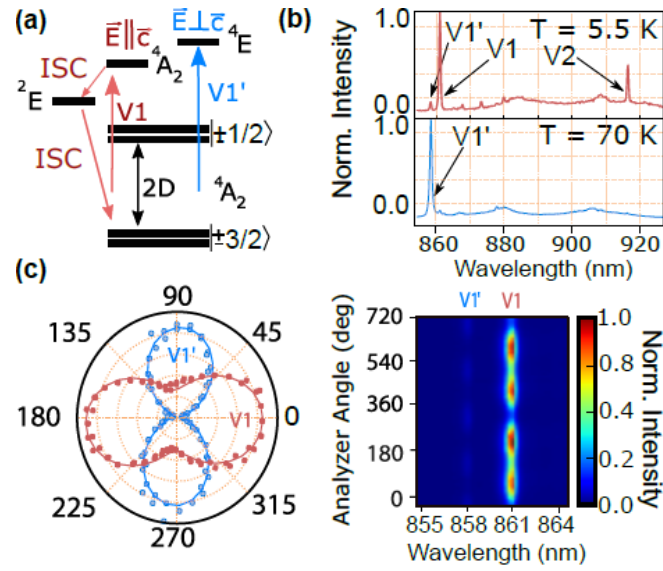


FIG. 1. (a) The energy level scheme of the V1 center. (b) The PL spectrum of a V_{Si} ensemble at 5.5 K and 70 K. (c) The optical polarization of the V1/V1' transitions at the sample orientation in which the c-axis is perpendicular to the laser incident direction at 5.5K. Left: the polar plot of the normalized V1 and V1' intensities. 0° , equivalently 180° , corresponds to the c-axis orientation. Right: the density plot showing the absolute intensities of the V1/V1' ZPLs.

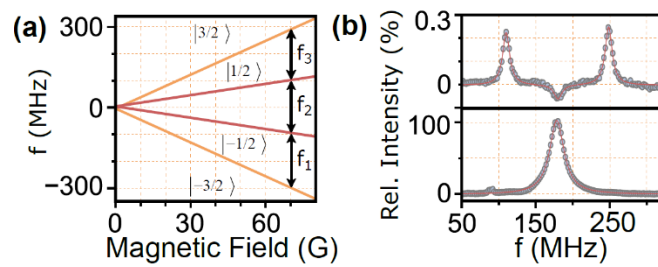


FIG. 2. (a) Zeeman effect of the spin $3/2$ ground state of the V1 center for $B_0 Pc$. f_1 , f_2 , and f_3 represent possible resonant transitions. (b) Upper panel: an ensemble ODMR spectrum with a 730 nm laser at 60 G. Lower panel: the ODMR with a laser resonant to V1, 861 nm.

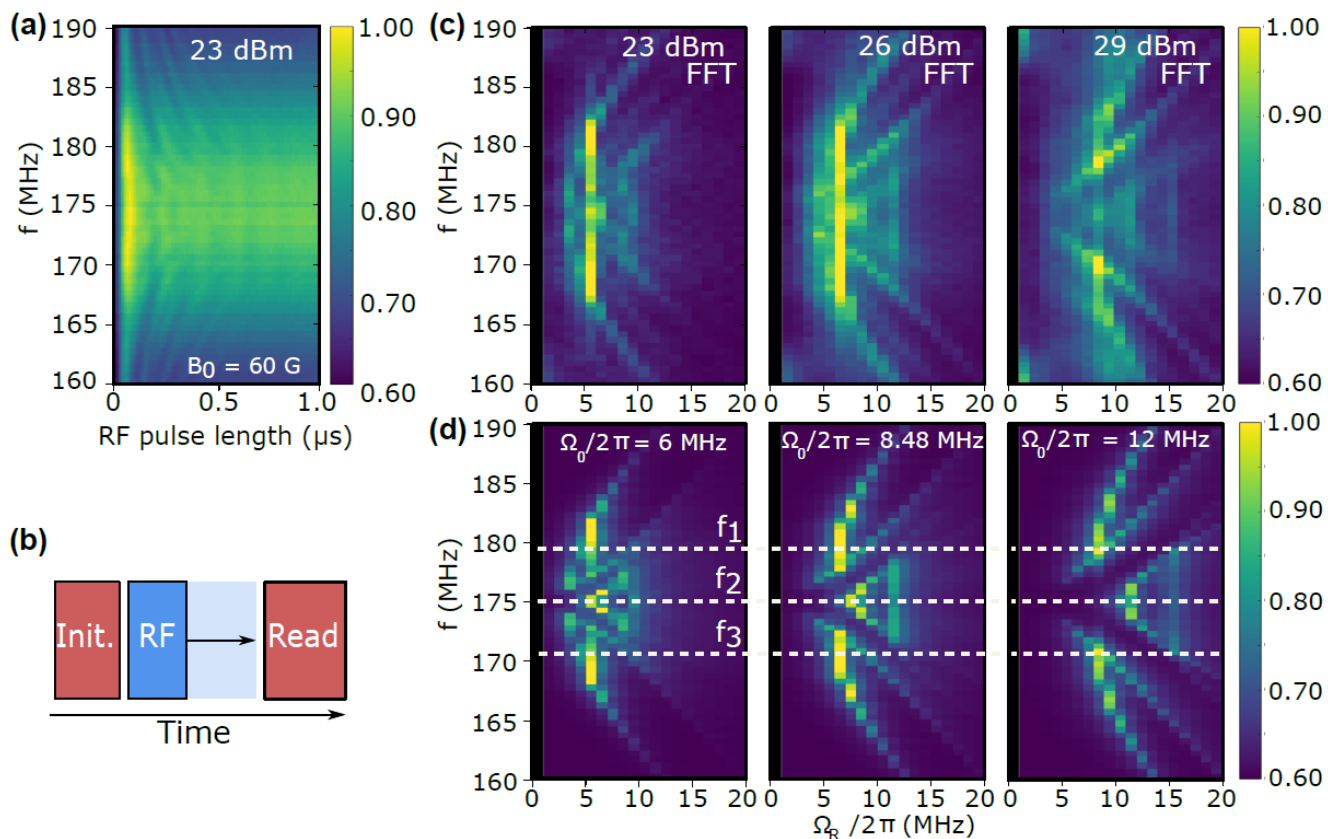


FIG. 3. (a) Rabi measurement with detuned RF driving frequencies. (b) Pulse scheme for a Rabi measurement. The first laser pulse (Init.) is polarizing the spin state. The RF pulse is manipulating the spin state followed by the last laser pulse (Read) for the spin state readout. (c) Fast Fourier transformed Rabi oscillations at different RF powers. (d) Simulated Rabi oscillations. The dotted lines indicate three resonant RF frequencies shown in Fig. 2(a). The strong zero frequency intensities in both (C) and (D) are removed for better distinguishability of the Rabi frequencies.

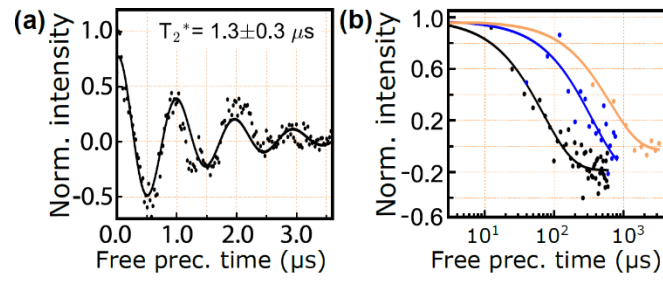


FIG. 4. (a) Ramsey measurement at $B_0 = 1000$ G. (b) The spin decoherence measured at $B_0 = 1000$ G by Hahn-Echo (black) and XY-8 dynamic decoupling (blue: $N=10$, Orange: $N=50$). See the Supplemental Materials for the used pulse sequence [36].

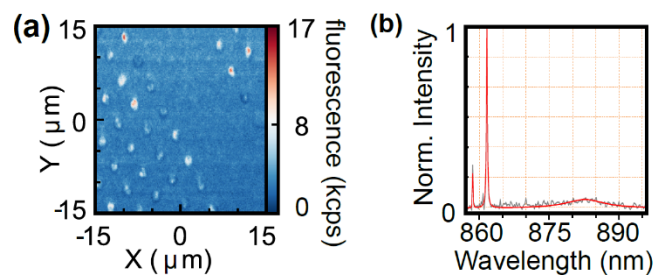


FIG. 5. (a) Confocal fluorescence raster scan showing single silicon vacancy V1 and V2 centers in SiC nanopillars at 4K. (b) A single V1 defect PL spectrum with the V1'/V1 ZPLs at 858 and 861 nm, respectively.

*sangyun.lee@kist.re.kr

†These authors contributed equally.

- [1] G. Balasubramanian, P. Neumann, D. Twitchen, M. Markham, R. Kolesov, N. Mizuochi, J. Isoya, J. Achard, J. Beck, J. Tissler, V. Jacques, P. R. Hemmer, F. Jelezko, and J. Wrachtrup, Ultralong Spin Coherence Time in Isotopically Engineered Diamond. **8**, 383 (2009).
- [2] T. Häberle, D. Schmid-Lorch, K. Karrai, F. Reinhard, and J. Wrachtrup, High-Dynamic-Range Imaging of Nanoscale Magnetic Fields Using Optimal Control of a Single Qubit **111**, 170801 (2013).
- [3] D. D. Awschalom, L. C. Bassett, A. S. Dzurak, E. L. Hu, and J. R. Petta, Quantum Spintronics: Engineering and Manipulating Atom-Like Spins in Semiconductors **339**, 1174 (2013).
- [4] N. Aslam, M. Pfender, P. Neumann, R. Reuter, A. Zappe, F. Fávoro de Oliveira, A. Denisenko, H. Sumiya, S. Onoda, J. Isoya, and J. Wrachtrup, Nanoscale Nuclear Magnetic Resonance with Chemical Resolution 10.1126/science.aam8697 (2017).
- [5] S. Yang, Y. Wang, D. D. B. Rao, T. Hien Tran, A. S. Momenzadeh, M. Markham, D. J. Twitchen, P. Wang, W. Yang, R. Stöhr, P. Neumann, H. Kosaka, and J. Wrachtrup, High-Fidelity Transfer and Storage of Photon States in a Single Nuclear Spin **10**, 507 (2016).
- [6] D. D. B. Rao, S. Yang, and J. Wrachtrup, Generation of Entangled Photon Strings Using NV Centers in Diamond **92**, 81301 (2015).
- [7] D. A. Golter, T. Oo, M. Amezcua, K. A. Stewart, and H. Wang, Optomechanical Quantum Control of a Nitrogen-Vacancy Center in Diamond **116**, 143602 (2016).
- [8] G. Waldherr, Y. Wang, S. Zaiser, M. Jamali, T. Schulte-Herbrüggen, H. Abe, T. Ohshima, J. Isoya, J. F. Du, P. Neumann, and J. Wrachtrup, Quantum Error Correction in a Solid-State Hybrid Spin Register. **506**, 204 (2014).
- [9] L. Li, T. Schröder, E. H. Chen, M. Walsh, I. Bayn, J. Goldstein, O. Gaathon, M. E. Trusheim, M. Lu, J. Mower, M. Cotlet, M. L. Markham, D. J. Twitchen, and D. Englund, Coherent Spin Control of a Nanocavity-Enhanced Qubit in Diamond. **6**, 6173 (2015).
- [10] T. Kimoto and J. A. Cooper, *Fundamentals of Silicon Carbide Technology: Growth, Characterization, Devices and Applications* (John Wiley & Sons, Singapore, 2014).
- [11] L. P. Yang, C. Burk, M. Widmann, S. Y. Lee, J. Wrachtrup, and N. Zhao, Electron Spin Decoherence in Silicon Carbide Nuclear Spin Bath **90**, 241203 (2014).
- [12] H. Seo, A. L. Falk, P. V Klimov, K. C. Miao, G. Galli, and D. D. Awschalom, Quantum Decoherence Dynamics of Divacancy Spins in Silicon Carbide **7**, 12935 (2016).
- [13] D. Simin, H. Kraus, A. Sperlich, T. Ohshima, G. V Astakhov, and V. Dyakonov, Locking of Electron Spin Coherence above 20 Ms in Natural Silicon Carbide **95**, 161201 (2017).
- [14] E. Sörman, N. Son, W. Chen, O. Kordina, C. Hallin, and E. Janzén, Silicon Vacancy Related Defect in 4H and 6H SiC **61**, 2613 (2000).
- [15] W. F. Koehl, B. B. Buckley, F. J. Heremans, G. Calusine, and D. D. Awschalom, Room Temperature Coherent Control of Defect Spin Qubits in Silicon Carbide. **479**, 84 (2011).
- [16] V. A. Soltamov, B. V. Yavkin, D. O. Tolmachev, R. A. Babunts, A. G. Badalyan, V. Y. Davydov, E. N. Mokhov, I. I. Proskuryakov, S. B. Orlinskii, and P. G. Baranov, Optically Addressable Silicon Vacancy-Related Spin Centers in Rhombic Silicon Carbide with High Breakdown Characteristics and ENDOR Evidence of Their Structure **115**, 247602 (2015).

- [17] D. Christle, A. Falk, P. Andrich, P. V. Klimov, J. Ul Hassan, N. T. Son, E. Janzén, T. Ohshima, and D. D. Awschalom, Isolated Electron Spins in Silicon Carbide with Millisecond-Coherence Times **14**, 160 (2015).
- [18] M. Widmann, S.-Y. Lee, T. Rendler, N. T. Son, H. Fedder, S. Paik, L.-P. Yang, N. Zhao, S. Yang, I. Booker, A. Denisenko, M. Jamali, S. A. Momenzadeh, I. Gerhardt, T. Ohshima, A. Gali, E. Janzén, and J. Wrachtrup, Coherent Control of Single Spins in Silicon Carbide at Room Temperature. **14**, 164 (2015).
- [19] K. Lee, L. Dang, G. Watkins, and W. Choyke, Optically Detected Magnetic Resonance Study of SiC: Ti **32**, 2273 (1985).
- [20] W. F. Koehl, B. Diler, S. J. Whiteley, A. Bourassa, N. T. Son, E. Janzén, and D. D. Awschalom, Resonant Optical Spectroscopy and Coherent Control of Cr⁴⁺ Spin Ensembles in SiC and GaN **95**, 35207 (2017).
- [21] E. Janzén, A. Gali, P. Carlsson, A. Gällström, B. Magnusson, and N. T. T. Son, The Silicon Vacancy in SiC **404**, 4354 (2009).
- [22] D. J. Christle, P. V. Klimov, C. F. Casas, K. Szász, V. Ivády, V. Jokubavicius, M. Syväjärvi, W. F. Koehl, T. Ohshima, and N. T. Son, Isolated Spin Qubits in SiC with a High-Fidelity Infrared Spin-to-Photon Interface **7**, 21046 (2017).
- [23] H. Kraus, V. a. Soltamov, D. Riedel, S. Váth, F. Fuchs, a. Sperlich, P. G. Baranov, V. Dyakonov, and G. V. Astakhov, Room-Temperature Quantum Microwave Emitters Based on Spin Defects in Silicon Carbide **10**, 157 (2013).
- [24] M. Veldhorst, C. H. Yang, J. C. C. Hwang, W. Huang, J. P. Dehollain, J. T. Muhonen, S. Simmons, A. Laucht, F. E. Hudson, K. M. Itoh, A. Morello, and A. S. Dzurak, A Two-Qubit Logic Gate in Silicon **526**, 410 (2015).
- [25] T. Wimbauer, B. K. Meyer, A. Hofstaetter, A. Scharmann, and H. Overhof, Negatively Charged Si Vacancy in 4H SiC: A Comparison between Theory and Experiment **56**, 7384 (1997).
- [26] N. Mizuochi, S. Yamasaki, H. Takizawa, N. Morishita, T. Ohshima, H. Itoh, and J. Isoya, Continuous-Wave and Pulsed EPR Study of the Negatively Charged Silicon Vacancy with S=3/2 and C_{3v} Symmetry in N-Type 4H-SiC **66**, 235202 (2002).
- [27] M. Niethammer, M. Widmann, S.-Y. Lee, P. Stenberg, O. Kordina, T. Ohshima, N. T. Son, E. Janzén, and J. Wrachtrup, Vector Magnetometry Using Silicon Vacancies in 4H-SiC Under Ambient Conditions **6**, 34001 (2016).
- [28] N. M. Atherton, *Principles of Electron Spin Resonance* (Ellis Horwood Series in Physical Chemistry, 1993).
- [29] O. Soykal, P. Dev, and S. E. Economou, Silicon Vacancy Center in 4H -SiC: Electronic Structure and Spin-Photon Interfaces **93**, 81207 (2016).
- [30] S. E. Economou and P. Dev, Spin-Photon Entanglement Interfaces in Silicon Carbide Defect Centers **27**, (2016).
- [31] J. Michl, T. Teraji, S. Zaiser, I. Jakobi, G. Waldherr, F. Dolde, P. Neumann, M. W. Doherty, N. B. Manson, J. Isoya, and J. Wrachtrup, Perfect Alignment and Preferential Orientation of Nitrogen-Vacancy Centers during Chemical Vapor Deposition Diamond Growth on (111) Surfaces **104**, 102407 (2014).
- [32] A. L. Falk, B. B. Buckley, G. Calusine, W. F. Koehl, V. V. Dobrovitski, A. Politi, C. A. Zorman, P. X.-L. Feng, D. D. Awschalom, V. Viatcheslav, A. Politi, C. A. Zorman, X. Feng, and D. D. Awschalom, Polytype Control of Spin Qubits in Silicon Carbide. **4**, 1819 (2013).
- [33] P. Baranov, A. Bundakova, A. Soltamova, S. Orlinskii, I. Borovykh, R. Zondervan, R. Verberk, and J.

- Schmidt, Silicon Vacancy in SiC as a Promising Quantum System for Single-Defect and Single-Photon Spectroscopy **83**, 125203 (2011).
- [34] S. G. Carter, O. O. Soykal, P. Dev, S. E. Economou, and E. R. Glaser, Spin Coherence and Echo Modulation of the Silicon Vacancy in 4H-SiC at Room Temperature **92**, 161202 (2015).
- [35] M. Radulaski, M. Widmann, M. Niethammer, J. L. Zhang, S.-Y. Lee, T. Rendler, K. G. Lagoudakis, N. T. Son, E. Janzen, T. Ohshima, J. Wrachtrup, and J. Vučković, Scalable Quantum Photonics with Single Color Centers in Silicon Carbide **17**, 1782 (2017).
- [36] *See Supplemental Material for Further Details* (n.d.).
- [37] D. O. Bracher, X. Zhang, and E. L. Hu, Selective Purcell Enhancement of Two Closely Linked Zero-Phonon Transitions of a Silicon Carbide Color Center **114**, 4060 (2016).
- [38] M. Wagner, B. Magnusson, W. Chen, E. Janzén, E. Sörman, C. Hallin, and J. Lindström, Electronic Structure of the Neutral Silicon Vacancy in 4H and 6H SiC **62**, 555 (2000).
- [39] J. Oreg, F. T. Hioe, and J. H. Eberly, Adiabatic Following in Multilevel Systems **29**, 690 (1984).
- [40] C. Neill, P. Roushan, M. Fang, Y. Chen, M. Kolodrubetz, Z. Chen, A. Megrant, R. Barends, B. Campbell, B. Chiaro, A. Dunsworth, E. Jeffrey, J. Kelly, J. Mutus, P. J. J. O'Malley, C. Quintana, D. Sank, A. Vainsencher, J. Wenner, T. C. White, A. Polkovnikov, and J. M. Martinis, Ergodic Dynamics and Thermalization in an Isolated Quantum System **12**, 1037 (2016).
- [41] M. V. Berry, Transitionless Quantum Driving **42**, 365303 (2009).
- [42] B. B. Zhou, A. Baksic, H. Ribeiro, C. G. Yale, F. J. Heremans, P. C. Jerger, A. Auer, G. Burkard, A. A. Clerk, and D. D. Awschalom, Accelerated Quantum Control Using Superadiabatic Dynamics in a Solid-State Lambda System **13**, 330 (2016).
- [43] A. M. Souza, G. A. Álvarez, and D. Suter, Robust Dynamical Decoupling **370**, 4748 (2012).
- [44] P. V Klimov, A. L. Falk, D. J. Christle, V. V Dobrovitski, and D. D. Awschalom, Quantum Entanglement at Ambient Conditions in a Macroscopic Solid-State Spin Ensemble **1**, (2015).
- [45] E. Togan, Y. Chu, A. S. Trifonov, L. Jiang, J. Maze, L. Childress, M. V. G. Dutt, A. S. Sørensen, P. R. Hemmer, A. S. Zibrov, and M. D. Lukin, Quantum Entanglement between an Optical Photon and a Solid-State Spin Qubit. **466**, 730 (2010).
- [46] A. Alkauskas, B. B. Buckley, D. D. Awschalom, and C. G. Van De Walle, First-Principles Theory of the Luminescence Lineshape for the Triplet Transition in Diamond NV Centres **16**, 73026 (2014).
- [47] A. P. Magyar, D. Bracher, J. C. Lee, I. Aharonovich, and E. L. Hu, High Quality SiC Microdisk Resonators Fabricated from Monolithic Epilayer Wafers **104**, 51109 (2014).
- [48] N. H. Lindner and T. Rudolph, Proposal for Pulsed On-Demand Sources of Photonic Cluster State Strings **103**, 113602 (2009).